Supporting Information

Selective Electrochemical Reduction of CO_2 to CO on CuO/In_2O_3 Nanocomposite: Role of Oxygen Vacancies

Pinki Devi,[a] Karan Malik,[b] Ekta Arora,[a] Saswata Bhattacharya,[a] V. Kalendra,[c] K. V. Lakshmi,[c] Anil Verma[b] and Jitendra P. Singh[a*]

[a]Department of Physics, Indian Institute of Technology Delhi, Hauz Khas, New Delhi 110016, India

[b]Department of Chemical Engineering, Indian Institute of Technology Delhi, Hauz Khas, New Delhi 110016, India

[c]Department of Chemistry and Chemical Biology and The Baruch '60 Center for Biochemical Solar Energy Research, Rensselaer Polytechnic Institute, Troy, NY 12180, U. S. A.

***Corresponding author: jpsingh@physics.iitd.ac.in**

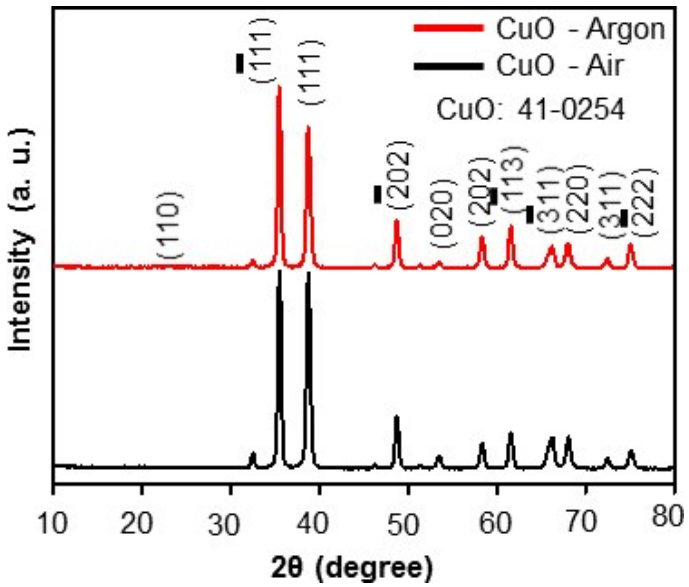

Fig. S1 XRD of CuO nanorods synthesized in air and argon environment.

Table S1. Crystallite size of CuO nanorods and CuO/In_2O_3 nanocomposites, synthesized both in air and argon environment.

Samples	CuO		5% CuO/ In_2O_3		10% CuO/ In_2O_3		15% CuO/In_2O_3	
Calcined Environment	Air	Argon	Air	Argon	Air	Argon	Air	Argon
Crystallite Size (nm)	19.58	20.20	14.56	11.39	14.73	17.53	15.83	15.80

The morphology of the 5%, 10% and 15% CuO/In_2O_3 nanocomposites that were synthesized in either in air or argon are shown in Fig. S2a-f. Fig. S2a-c and Fig. S2d-f depict the one-dimensional (1D) morphology of the nanocomposites in air and argon, respectively. Fig. S2g-h depicts the 1D morphology of bare CuO synthesized in air and argon, respectively. The insets represent the corresponding micrographs at higher magnification. The 5% CuO/In_2O_3 nanocomposites synthesized in air display a fiber-like morphology (Fig. S2a), while the fibers appear to be stacked as bundles of ~ 2 μm diameter when same sample was prepared in an argon environment (Fig. S2d). The individual nanorods with an aspect ratio of approximately 4 were observed for the 10% CuO/In_2O_3 nanocomposite prepared in air (Fig. S2b). In contrast, the nanorods were agglomerated when the same sample prepared in the presence of argon (Fig. S2e). The fiber-like morphology (Fig. S2c) was packed into a sheath of bundles (Fig. S2f) in the case of the 15% CuO/In_2O_3 nanocomposite.

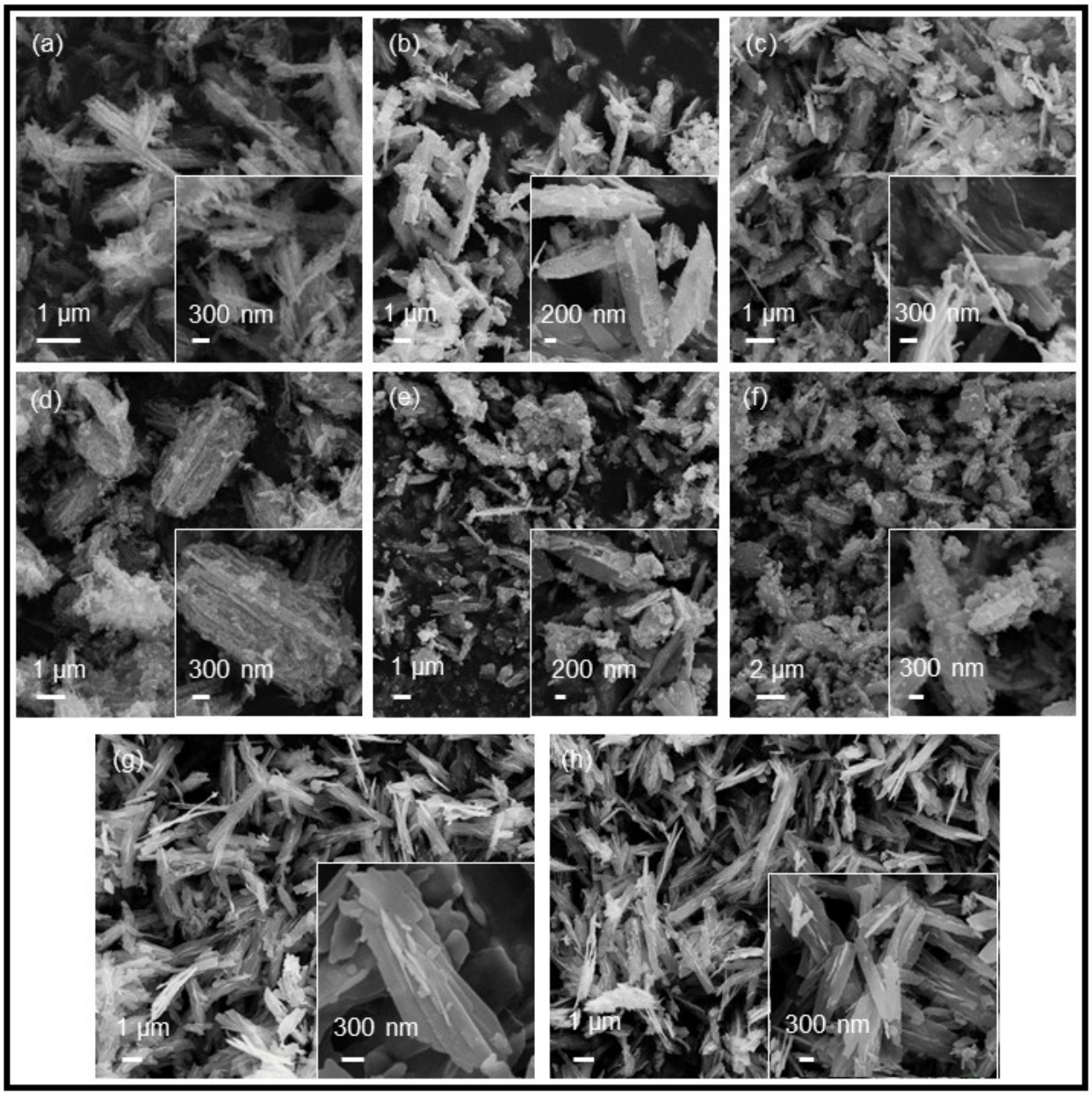

Fig. S2 SEM images of (a, d) 5%, (b, e) 10%, (c, f) 15% CuO/In_2O_3 nanocomposite (g-h) CuO nanorods synthesized in air and argon environments, respectively. Insets represent their corresponding higher magnification images.

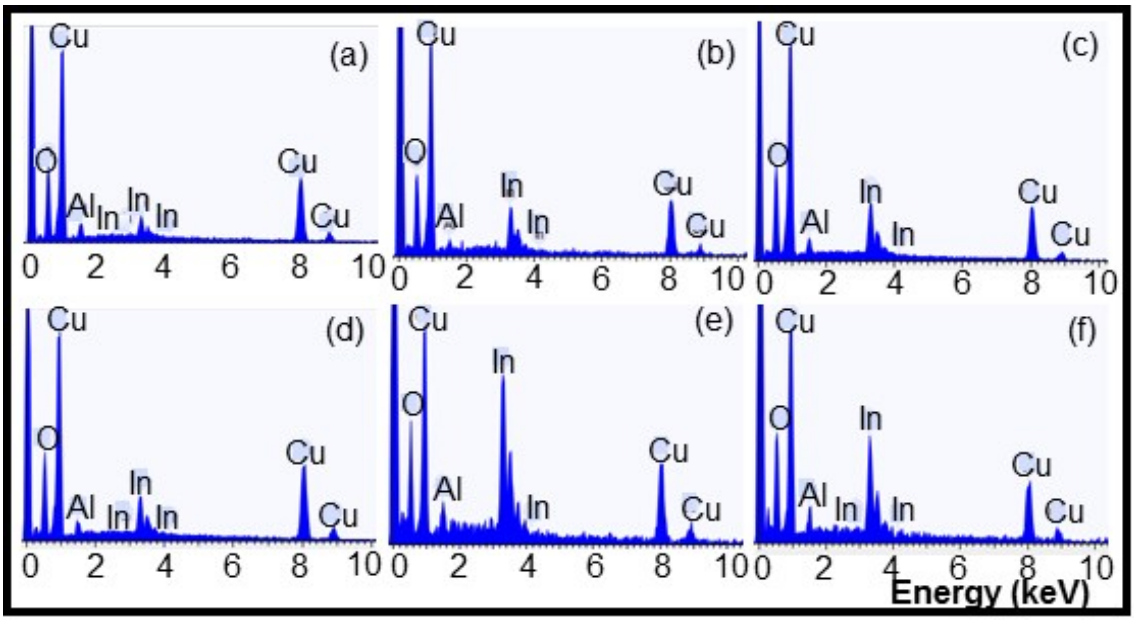

Fig. S3 EDX spectra of (a, d) 5%, (b, e) 10%, (c, f) 15% CuO/In_2O_3 nanocomposite synthesized in air and argon environments, respectively.

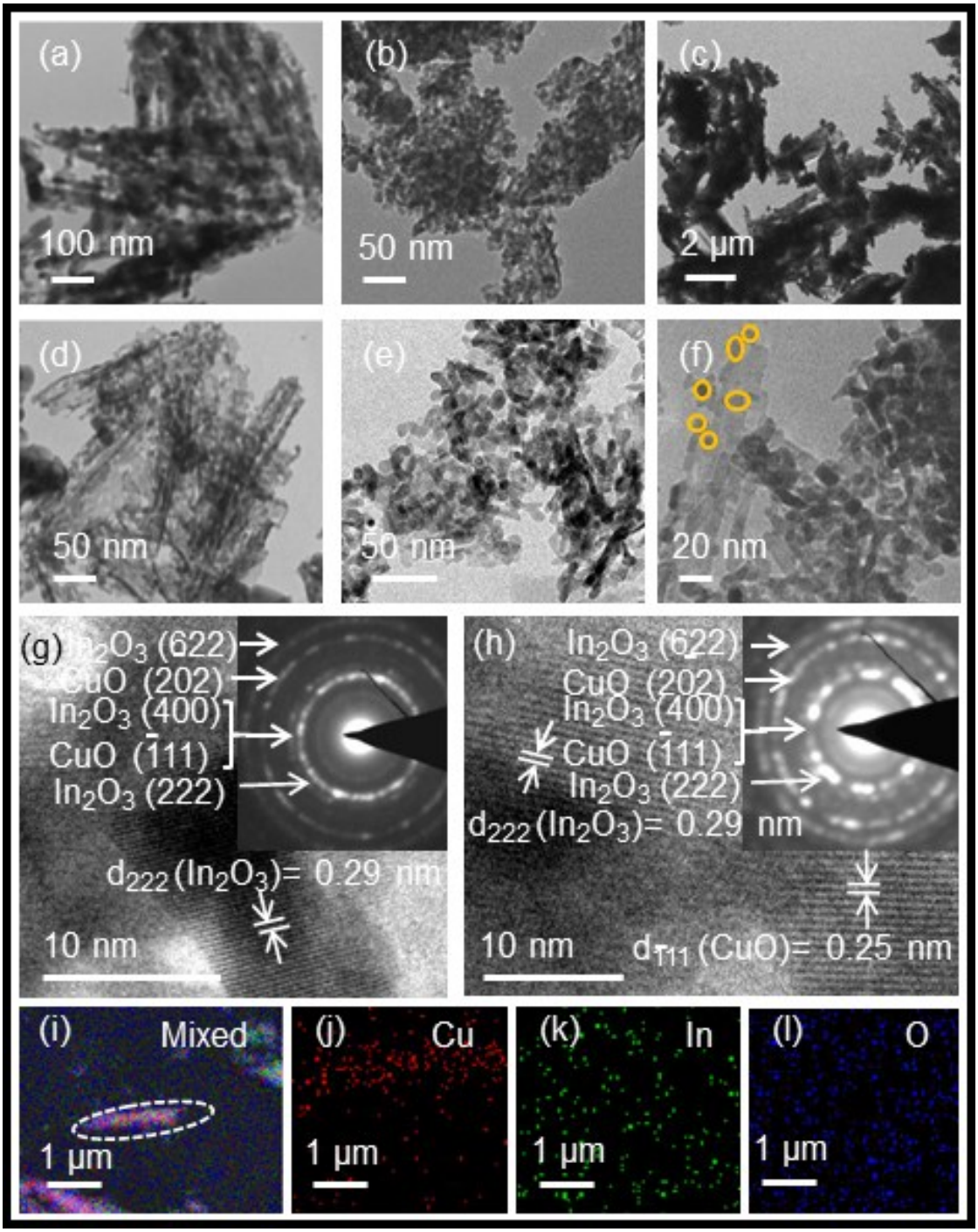

Fig. S4 TEM images of (a, d) 5%, (b, e) 10%, (c, f) 15% CuO/In_2O_3 nanocomposite synthesized in air and argon environments, respectively. HRTEM images of 10% CuO/In_2O_3 nanocomposite synthesized in (g) air and (h) argon environments. Insets of (g-h) represent corresponding SAED patterns. Elemental mapping images of (i) mixed, (j) Cu, (k) In and (l) O elements in 10% CuO/In_2O_3 nanocomposite synthesized under argon environment.

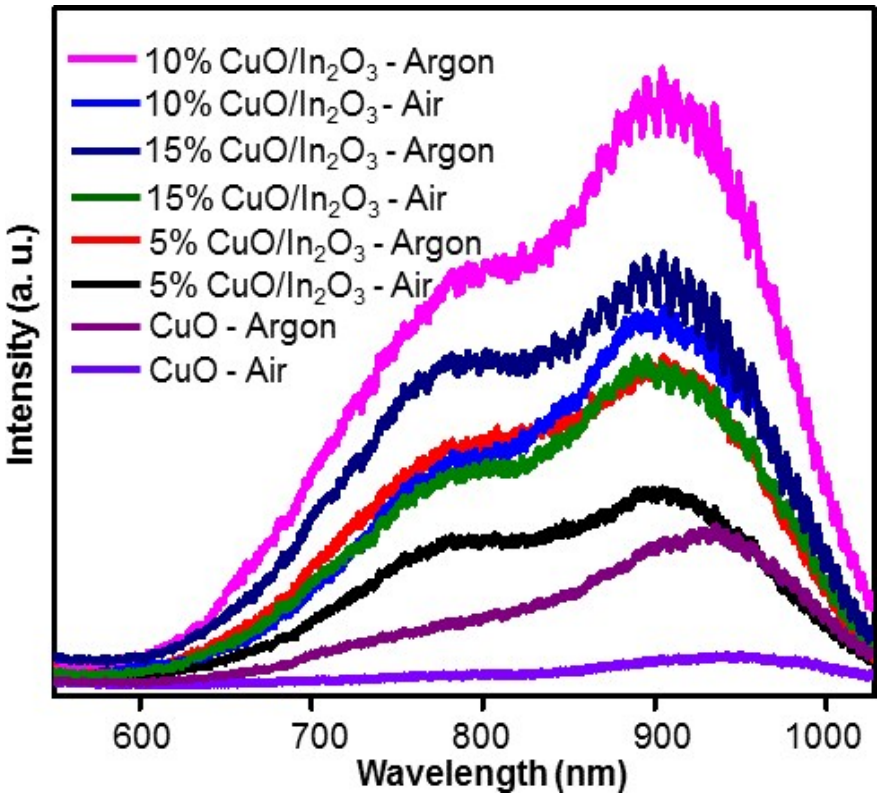

Fig. S5 PL spectra of CuO nanorods and CuO/In_2O_3 nanocomposites synthesized in air and argon environment.

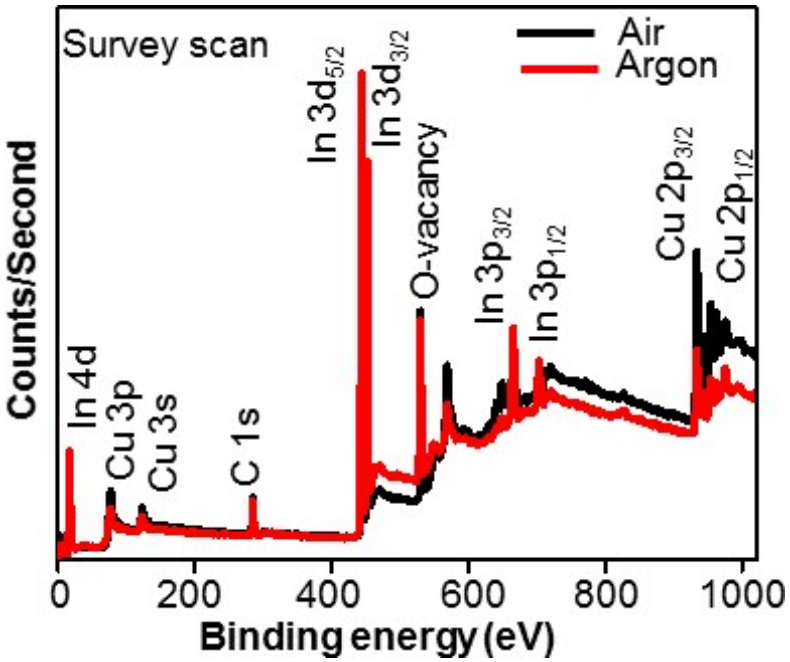

Fig. S6 XPS survey scan of 10% CuO/In_2O_3 nanocomposites synthesized both in air and argon environment.

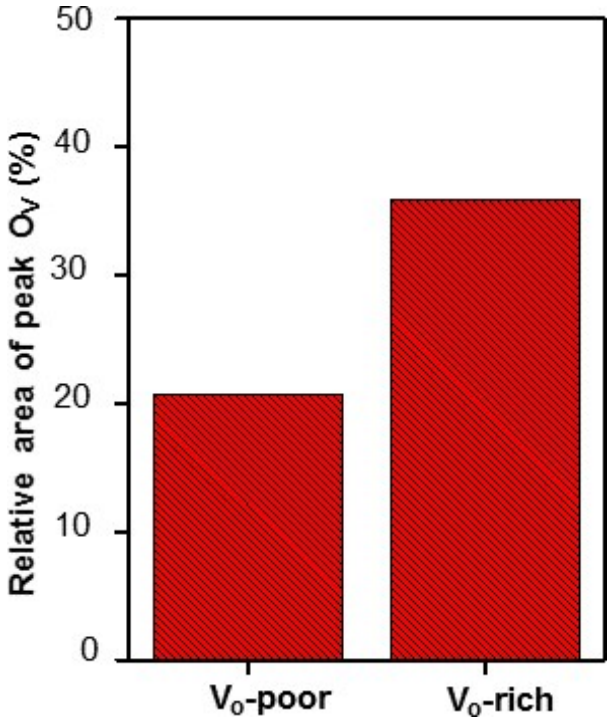

Fig. S7 Relative area of oxygen vacancy peak (O_V) in CuO/In_2O_3 nanocomposites synthesized in air and argon environment.

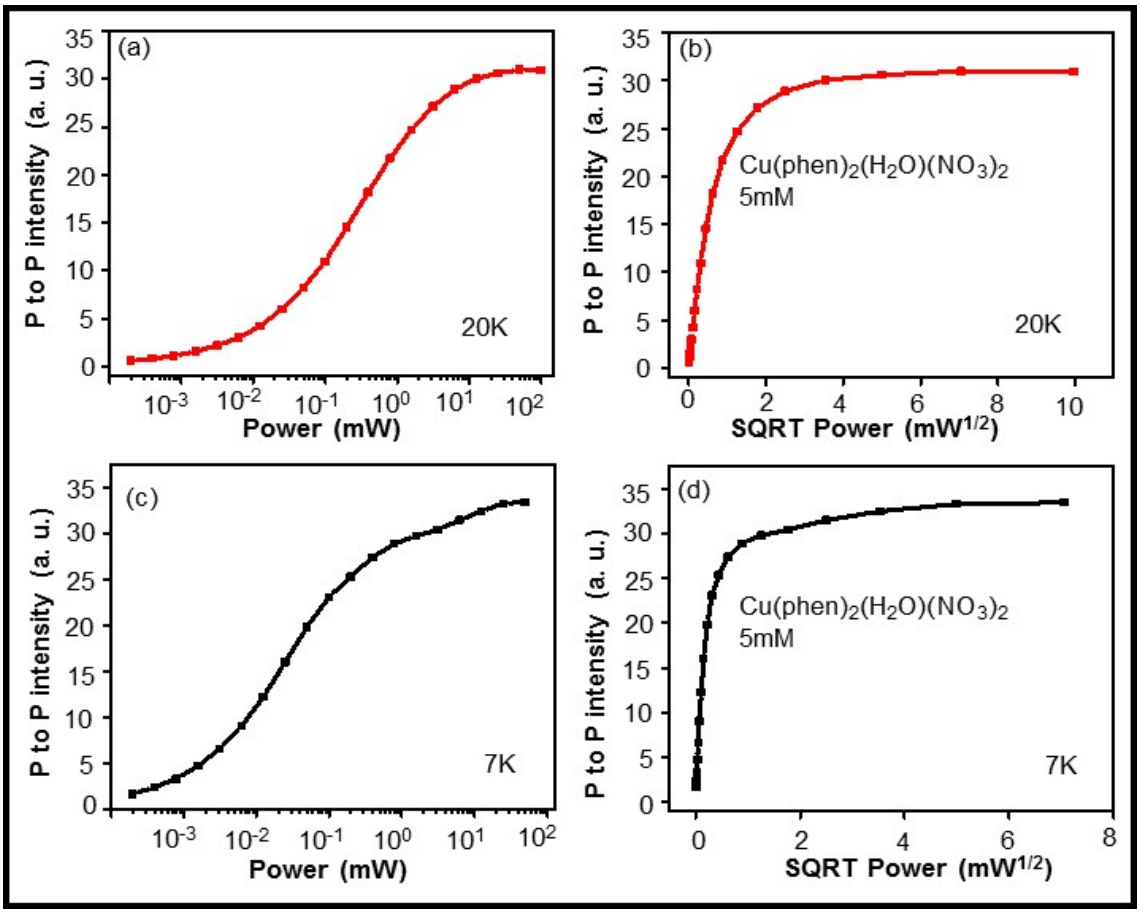

Fig. S8. Microwave power saturation EPR spectra of Cu saturation at (a and b) 20 K and (c and d) 7K of CuO/In_2O_3 nanocomposite.

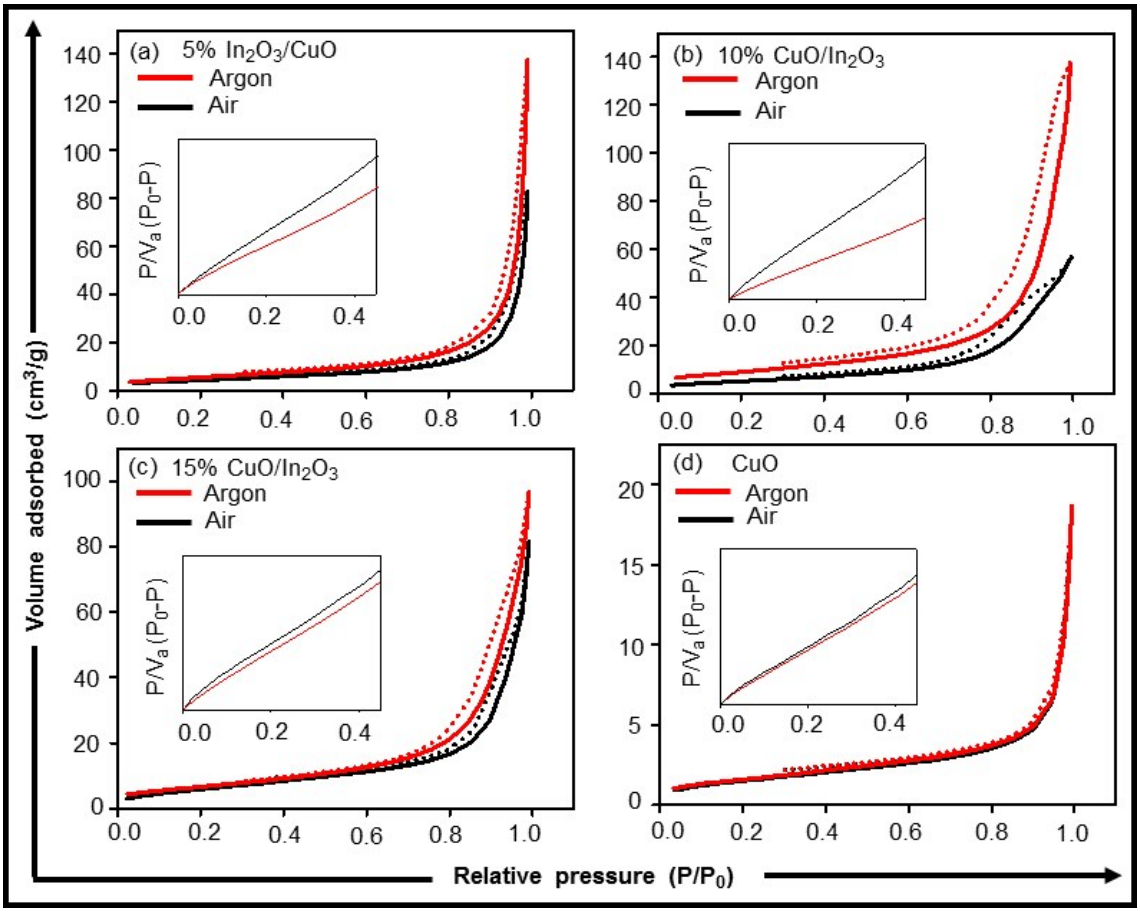

Fig. S9. BET surface area measurement (a) 5% CuO/In_2O_3 (b)10% CuO/In_2O_3 (c) 15% CuO/In_2O_3 nanocomposites (d) CuO nanorods synthesized in air and argon environment.

Table S2. BET surface area measurements of various CuO/In_2O_3 nanocomposites shown below:

Samples	calcined environment	BET surface area (m^2/g)	Mean pore diameter (nm)	Pore volume (cm^3/g)
5% CuO/In_2O_3 nanocomposite	Air	15.536	32.714	0.1271
	Argon	20.38	40.776	0.2078
10% CuO/In_2O_3 nanocomposite	Air	18.56	18.298	0.0849
	Argon	32.429	23.938	0.1941
15% CuO/In_2O_3 nanocomposite	Air	22.87	22.053	0.1261
	Argon	24.53	24.201	0.1484
CuO nanorods	Air	5.58	18.829	0.0262
	Argon	5.84	17.553	0.0256

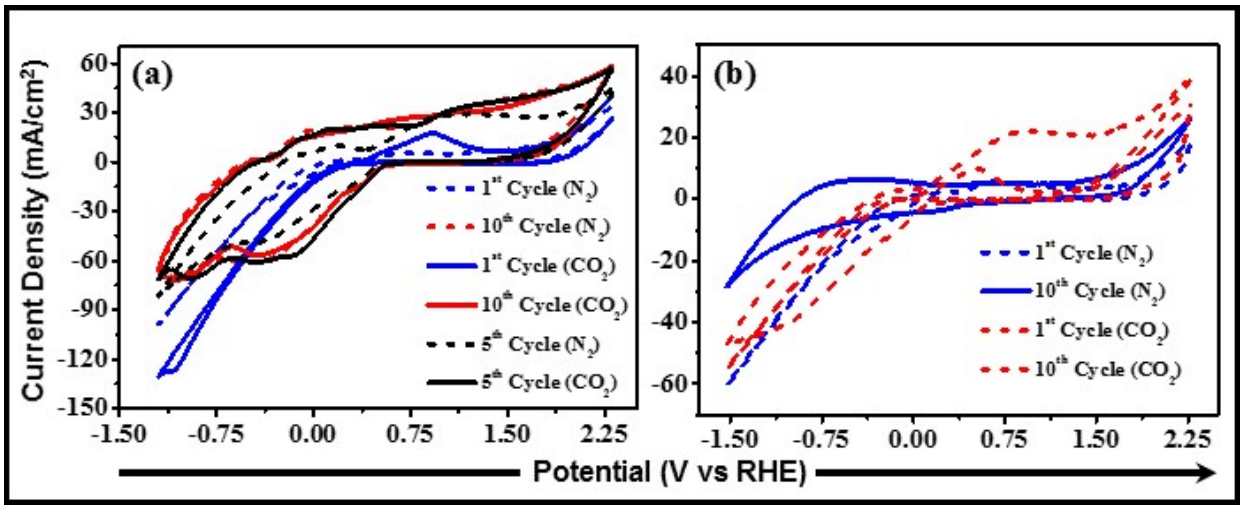

Fig. S10 Cyclic voltammetry of (a) 5% CuO/In_2O_3 (Argon) and (b) 10% CuO/In_2O_3 (Argon)

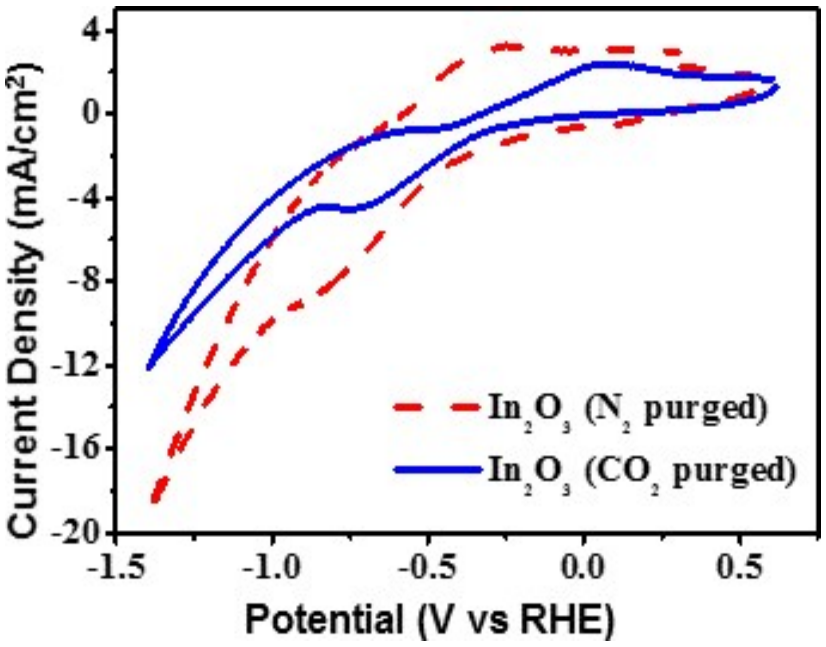

Fig. S11 Cyclic voltammetry of In_2O_3 nanoparticles in 0.1M $KHCO_3$.

Table S3. Chronoamperometry results of In_2O_3.

Potential (V *vs.* RHE)	FE_H (%)	FE_{CO} (%)	J (mA/cm^2)
-0.395	0.00	0.00	0.15
-0.645	49.3	23.5	0.61
-0.895	34.4	8.9	6.67
-1.145	94.9	3.0	28.68

The gaseous product analysis for the chronoamperometry study of In_2O_3 is shown in the table S3. Since the total charge passed at -0.395V was only 1.24C. Thus, the entire charge was used up by the electrocatalyst for its own reduction and only traces of products were detected. At potentials -0.645 V and -0.895 V total gaseous product FE is 72.8% and 43.3%, this indicates that some of the charge was utilized to produce liquid products. At -1.145 V, HER overtakes the ERC and only H_2 was produced as the dominant product.

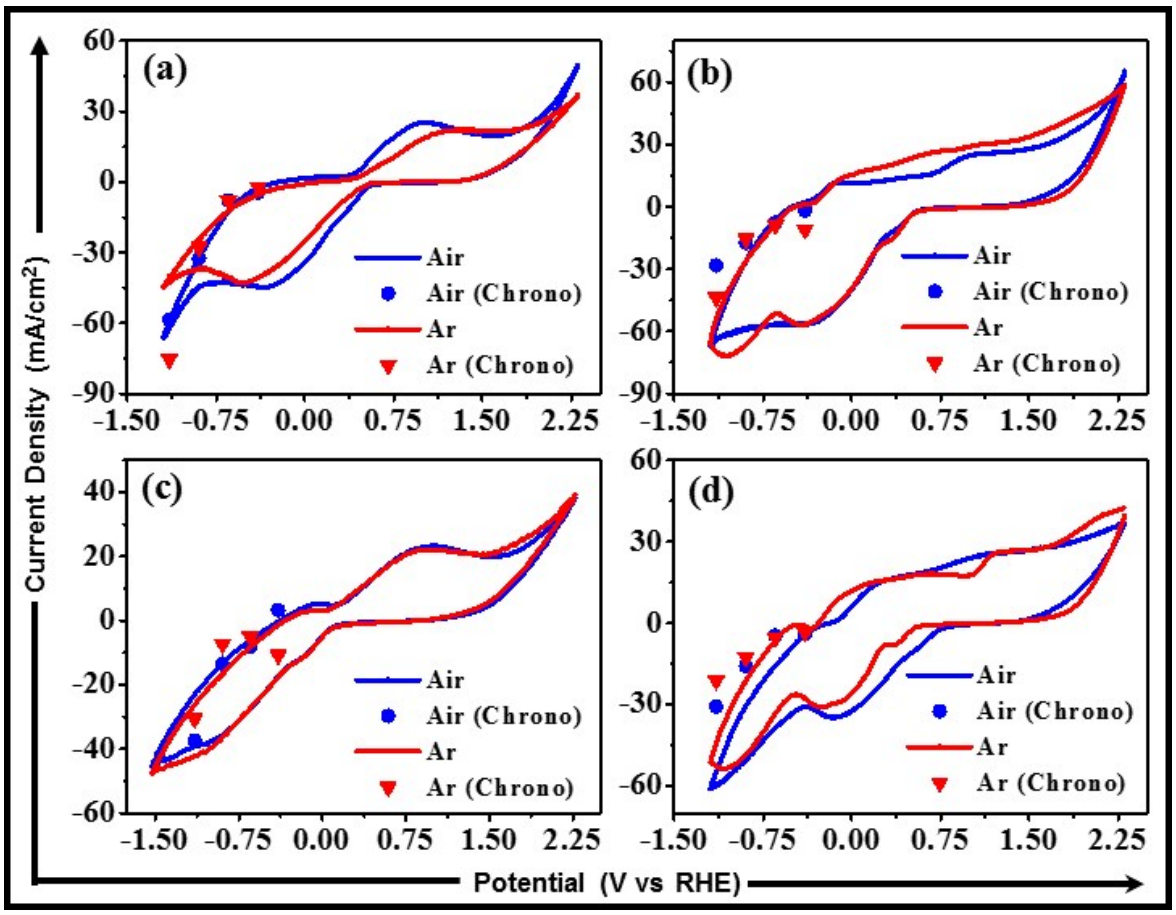

Fig. S12 Comparison between Cyclic voltammetry and Chronoamperometry current densities of (a) CuO (b) 5% CuO/In_2O_3 (c) 10% CuO/In_2O_3 and (d) 15% CuO/In_2O_3 nanocomposites.

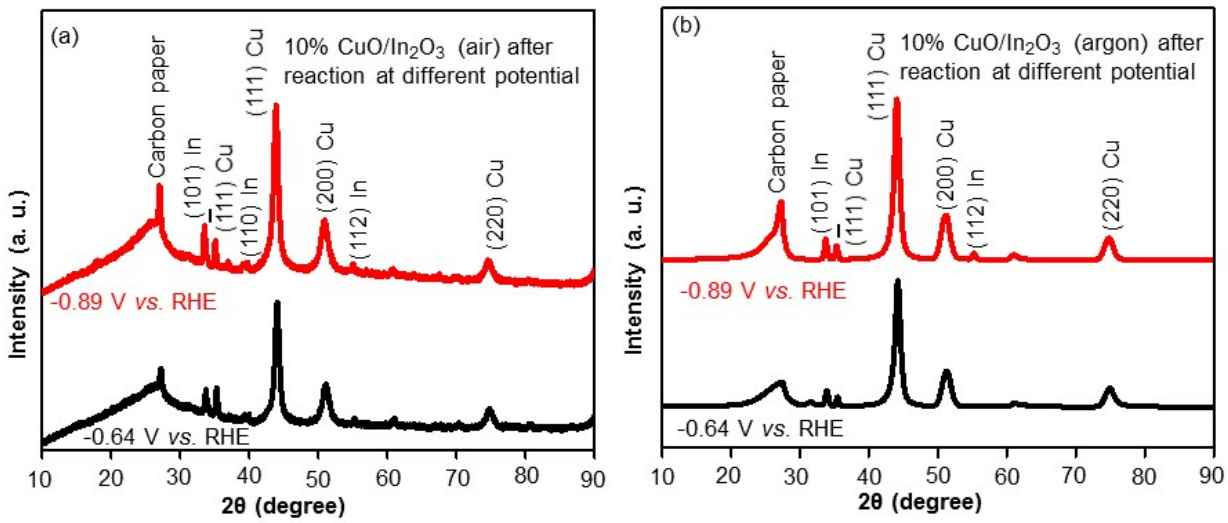

Fig. S13 XRD pattern of CuO/In_2O_3 (air) and CuO/In_2O_3 (argon) after 1 hour CO_2 reduction reaction at potential -0.64 and -0.89 V vs RHE.

The diffraction peak at 36.2°, 43.2°, 50.3° and 73.9º correspond to (-111), (111), (200) and (220) plane of Cu^0 with JCPDS no. 04-0836 and peak at 33.65°, 39.2°, and 55.23º correspond to (101), (110) and (112) plane of In^0 well indexed with JCPDS no. 05-0642. XRD pattern revealed that CuO/In_2O_3 nanocomposites after reaction are reduced to the metallic states of copper and indium.

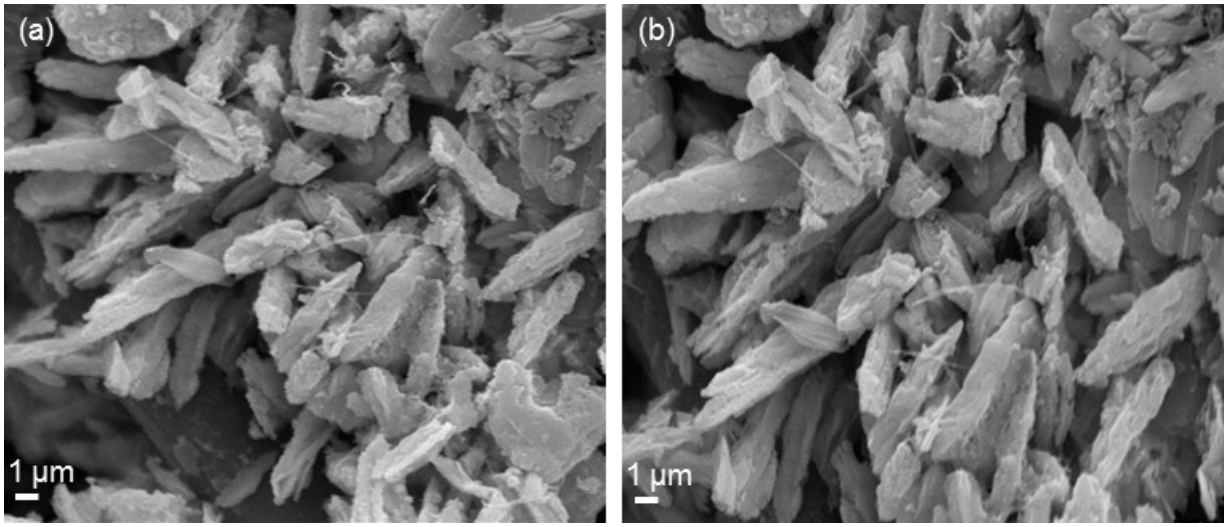

Fig. S14 SEM image of (a) CuO/In_2O_3 (air) and (b) CuO/In_2O_3 (argon) after reaction

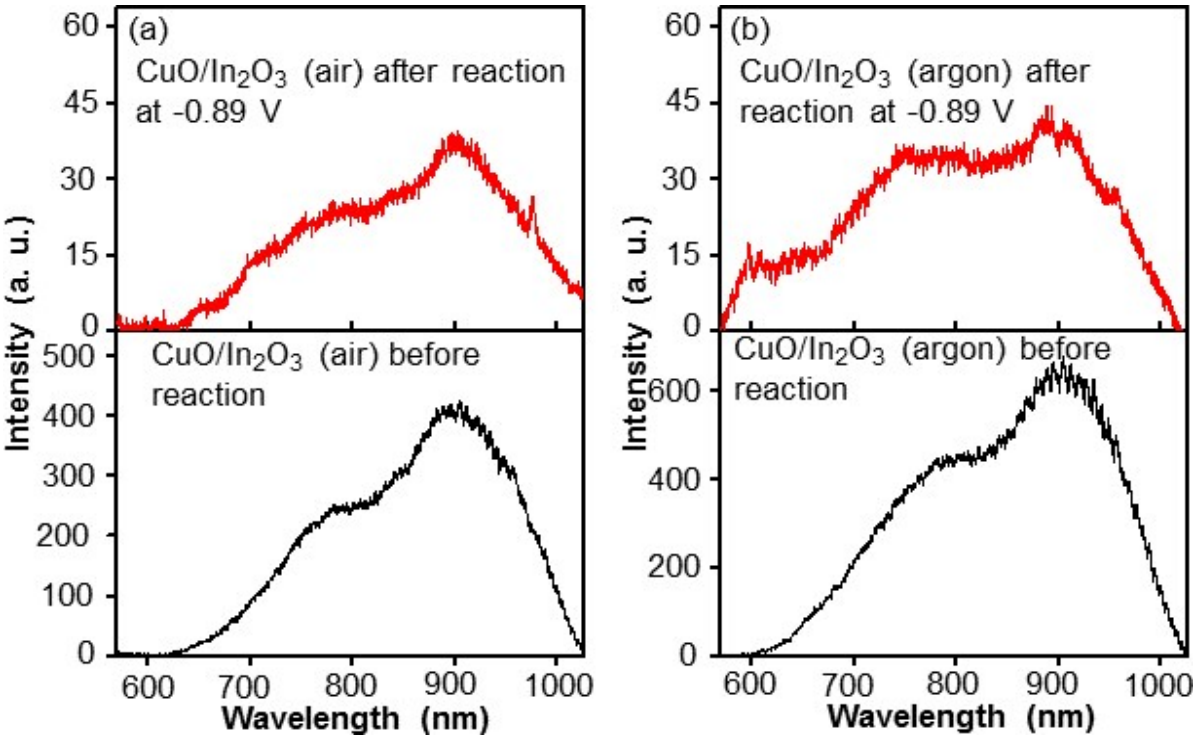

Fig. S15 PL spectra of (a) CuO/In_2O_3 (air) and (b) CuO/In_2O_3 (argon) before and after electrochemical reactions.

The stability of oxygen vacancies were confirmed by performing the post reaction PL measurement as shown in figure S15. The presence of defects in the PL spectra of both CuO/In_2O_3 (air and argon) before and after the reaction at potential -0.89V *vs* RHE, revealed the stability of oxygen vacancies defects during the electrochemical measurements of the catalyst. Figure S15 depicts the qualitative idea of oxygen vacancies concentration before and after CO_2 reduction reaction. Thus, V_o defects were stable in both CuO/In_2O_3 nanocomposites.